Eur. Phys. J. B **26**, 417–430 (2002)
DOI: 10.1140/epjb/e20020109

THE EUROPEAN PHYSICAL JOURNAL B
EDP Sciences

Slow relaxation experiments in disordered charge and spin density waves: collective dynamics of randomly distributed solitons

R. Mélin[1,a], K. Biljaković[2], J.C. Lasjaunias[1], and P. Monceau[1]

[1] Centre de Recherches sur les Très Basses Températures (CRTBT)[b], CNRS BP 166X, 38042 Grenoble Cedex, France
[2] Institute of Physics of the University, PO Box 304, 41001 Zagreb, Croatia, Yugoslavia

Received 12 December 2001

Abstract. We show that the dynamics of disordered charge density waves (CDWs) and spin density waves (SDWs) is a collective phenomenon. The very low temperature specific heat relaxation experiments are characterized by: (i) "interrupted" ageing (meaning that there is a maximal relaxation time); and (ii) a broad power-law spectrum of relaxation times which is the signature of a collective phenomenon. We propose a random energy model that can reproduce these two observations and from which it is possible to obtain an estimate of the glass cross-over temperature (typically $T_g \simeq 100-200$ mK). The broad relaxation time spectrum can also be obtained from the solutions of two microscopic models involving randomly distributed solitons. The collective behavior is similar to domain growth dynamics in the presence of disorder and can be described by the dynamical renormalization group that was proposed recently for the one dimensional random field Ising model [D.S. Fisher, P. Le Doussal, C. Monthus, Phys. Rev. Lett. **80**, 3539 (1998)]. The typical relaxation time scales like $\tau^{\rm typ} \sim \tau_0 \exp(T_g/T)$. The glass cross-over temperature T_g related to correlations among solitons is equal to the average energy barrier and scales like $T_g \sim 2x\xi_0\Delta$. x is the concentration of defects, ξ_0 the correlation length of the CDW or SDW and Δ the charge or spin gap.

PACS. 05.70.Ln Nonequilibrium and irreversible thermodynamics – 63.50.+x Vibrational states in disordered systems – 75.30.Fv Spin-density waves

1 Introduction

In spite of several decades of intensive experimental and theoretical works related to slow relaxation phenomena, important questions regarding the nature of the low temperature phase of spin glasses have remained unsolved. Replica symmetry breaking [1] and droplet theory [2,3] constitute two pictures that were already available in the 80's. It is a debated question to determine which of these two visions of the problem does apply to laboratory experiments (see for instance [4]). Recent "memory and chaos" experiments [5] suggest that a new type of droplet theory is needed but there exists unsolved questions that have been the subject of recent works (see for instance [6,7]). Other approaches have focussed on the description of out-of-equilibrium ageing dynamics in terms of generalized fluctuation-dissipation relations [8]. These ideas were originally developed in the context of spin glass models but have been used recently to discuss different systems such as domain growth dynamics or chaotic flows [9]. It has been shown recently in reference [10] that the long time dynamics of domain walls in the one dimensional (1D) random field Ising model (RFIM) could be described by a dynamical real space renormalization group (RG). The dynamical RG is similar to the Dasgupta-Ma RG [11] that was applied to the 1D random Ising model in a transverse magnetic field [12] and to the 1D random antiferromagnetic Heisenberg model [13]. The Dasgupta-Ma RG was also applied recently to many other random spin models [12–19]. The general purpose of our article is to use the dynamical RG to describe the long time collective dynamics of disordered charge density waves (CDWs) and spin density waves (SDWs).

Disordered quasi-one dimensional (quasi 1D) systems have known a renewed interest recently since the discovery of several inorganic low dimensional oxides such as $CuGeO_3$ [20–23] (a spin-Peierls compound), $PbNi_2V_2O_8$ [24] (a Haldane gap compound) and Y_2BaNiO_5 [25–30] (a Haldane gap compound). In these compounds the magnetic sites can be substituted with Zn

[a] e-mail: melin@polycnrs-gre.fr
[b] U.P.R. 5001 du CNRS, Laboratoire conventionné avec l'Université Joseph Fourier

(a non magnetic ion). These substitutions generate either 3D antiferromagnetism at low temperature (in the case of $CuGeO_3$ and $PbNi_2V_2O_8$) or strong 3D antiferromagnetic correlations (in the case of Y_2BaNiO_5). In these two types of low dimensional spin models, the non magnetic defects generate spin-1/2 moments out of the non magnetic ground state, either in the form of solitons in spin-Peierls systems [31–38], or in the form of "edge" spin-1/2 moments in Haldane gap systems [39–42]. The available theoretical description of these systems is based on the Dasgupta-Ma real space RG [11,43] describing non magnetic defects in 1D and quasi-1D geometries [30,44,45], and appears to be in good agreement with experiments.

It has been shown experimentally by some of the present authors that CDWs and SDWs present slow relaxation phenomena at very low temperature [46–48] under the form of what has been called "interrupted ageing" in the spin glass literature [49]. In fact there are two glass cross-over temperatures. One is due to the freezing of the CDW domains and is observed at relatively high temperature mainly in dielectric susceptibility experiments and is defined in the usual way for glassy systems as a separation of the so-called α- and β-relaxation processes (see Ref. [50]). We are interested here in slow relaxation phenomena occurring at lower temperature that were observed in temperature relaxation experiments [46–48]. Slow relaxation in disordered CDWs and SDWs and antiferromagnetism in the spin-Peierls compound $CuGeO_3$ have the common point that in both cases the physics is related to solitons having a slow dynamics in CDWs and SDWs (the microscopic time associated to the reversal of the soliton can be deduced from experiments and is $\tau_0 \simeq 1$ s – see Ref. [46–48]), and a fast dynamics in $CuGeO_3$ (no slow relaxation has been reported in ac-susceptibility experiments – see for instance [32] – and specific heat relaxation experiments [51]). The large value of τ_0 in CDWs and SDWs is due to energy barriers associated to the dynamics of individual solitons, not present in $CuGeO_3$. By comparison the microscopic time $\tau_0 \simeq 10^{-12}$ s in spin glasses corresponds to the reversal time of an individual spin. We show in this article from the analysis of quasi 1D strong pinning models that the dynamics of disordered CDWs and SDWs can be interpreted as a collective dynamics of randomly distributed solitons. This dynamics is similar to a domain growth dynamics in the presence of disorder in which a correlation length $\xi(t)$ is increasing with time. Larger objects have a slower relaxation because most of the time the energy barrier associated to a correlated pair of solitons that are close in space is larger than the energy barriers of the individual solitons.

It has been shown in references [52–56] from the analysis of a strong pinning model that there exist slow relaxation phenomena associated to independent strong pinning impurities in CDWs. It was also shown in reference [56] that the explanation based on independent impurities requires an artificially large concentration of impurities (one impurity per unit cell). It is therefore a relevant question to reexamine the experimental data and investigate new mechanisms responsible for slow relaxation in disordered CDWs and SDWs. More precisely we address the following questions:

1. In Section 2, we reexamine the slow relaxation experiments in CDWs and SDWs already presented in references [46–48] and find two features:
   (i) An "interrupted ageing" behavior (all relaxation times are smaller than a maximum relaxation time $\tau_{\max}$).
   (ii) A power-law relaxation spectrum signaling the presence of a broad distribution of relaxation times.
   The strong pinning model with independent impurities proposed in reference [56] has been successful to explain (i) but it does not explain (ii). In this article we look for a model that is consistent with (i) and (ii).
2. We propose in Section 3 a phenomenological random energy model (REM) that is compatible with the slow relaxation experiments.
3. We show in Section 4 that the experiments can be qualitatively described as being due to a collective behavior in a strong pinning model. A dynamical RG is used to describe the coupling between the solitonic deformations of the CDW at different impurities at variance with the previous model proposed in reference [56] where the solitonic defects are independent from each other.
4. We show in Section 5 that the experiments can also be qualitatively described by the disordered spin-Peierls model proposed in references [30,44,45].

2 Experiments

The specific heat and heat relaxation experiments (see Refs. [46–48]) have been performed at the CRTBT-Grenoble in a dilution cryostat over the typical temperature range 80 mK – 2 K on sample mass of a few hundreds mg. The experiments have been performed with a thermal transient technique, the sample being loosely connected to the regulated heat sink *via* a thermal link. This technique enables us to send energy in the sample for variable durations, from a pulse of a fraction of seconds up to a long "waiting time" of 24 h or more. For the thermal transient experiments reported here, the procedure is the following. Once the sample is in equilibrium with the heat bath at T_0, one increases slightly the sample temperature to $T_0 + \Delta T_0$, (with $\Delta T_0/T_0 \leq 10\%$) during a waiting time t_w. The energy source is switched off at t_w and the thermal transient $\Delta T(t, t_w)$ is recorded until the temperature has relaxed to the initial temperature T_0. t is the time elapsed since the waiting time t_w. The temperature relaxation $\Delta T(t, t_w)$ depends on the value of the waiting time (ageing behavior). If t_w is sufficiently large, $\Delta T(t, t_w)$ does not depend on t_w anymore ("interrupted ageing" behavior, see [49]). One can start a new run at T_0 with a different t_w. During a series of runs at different T_0 below 1 K, the sample is never

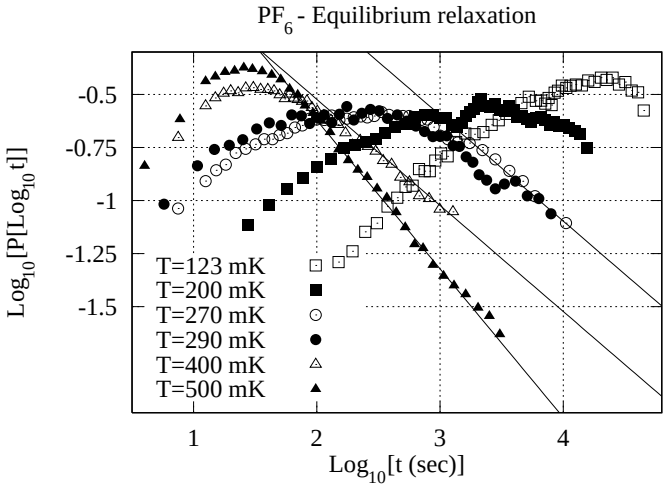

Fig. 1. Equilibrium relaxation time spectrum of the incommensurate SDW compound $(TMTSF)_2PF_6$. Equation (2) has been used to obtain the spectrum of relaxation times from the temperature relaxation signal. The waiting time is long enough so that thermal equilibrium has been reached for all temperatures except $T = 123$ mK. The long-time tail of the spectrum of relaxation times is well fitted by a power-law: $P_{\rm eq}(\log_{10} t) = 6\times t^{-0.7}$ for $T = 500$ mK; $P_{\rm eq}(\log_{10} t) = 3\times t^{-0.5}$ for $T = 400$ mK; $P_{\rm eq}(\log_{10} t) = 8 \times t^{-0.5}$ for $T = 270$ mK.

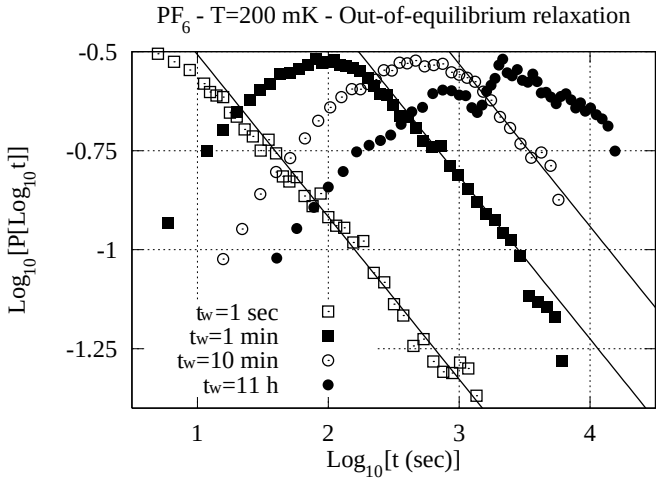

Fig. 2. Out-of-equilibrium relaxation time spectrum of the incommensurate SDW compound $(TMTSF)_2PF_6$ at the temperature $T = 200$ mK. Equation (2) has been used to obtain the spectrum of relaxation times from the temperature relaxation signal. Thermal equilibrium has been reached for the longest relaxation time ($t_w = 11$ h). The long-time tail of the spectrum of relaxation times is well fitted by a power-law: $P_{t_w}(\log_{10} t) = 2.6 \times t^{-0.41}$ for $t_w = 1$ sec; $P_{t_w}(\log_{10} t) = 5 \times t^{-0.41}$ for $t_w = 1$ min; $P_{t_w}(\log_{10} t) = 0.8 \times t^{-0.41}$ for $t_w = 10$ min.

re-heated above 1 – 2 K. Due to the exceptional stability of the cryostat, the reference temperature T_0 can be regulated within $\pm 2 \times 10^{-4}$ over several tens of hours.

We use a standard procedure to deduce a spectrum of relaxation times from the temperature relaxation $\Delta T(t, t_w)$:

$$\Delta T(t, t_w) = \int P_{t_w}(\log_{10} \tau) \mathrm{e}^{-t/\tau} \mathrm{d} \log_{10} \tau. \qquad (1)$$

An approximate expression for the spectrum of relaxation times can be obtained by replacing $\exp(-t/\tau)$ by the θ-function $\theta(\log_{10} \tau - \log_{10} t)$, which is justified for a broad relaxation time spectrum:

$$P_{t_w}(\log_{10} t) \simeq -\frac{\partial \Delta T(t, t_w)}{\partial \log_{10} t}\,. \qquad (2)$$

We first consider the incommensurate SDW compound $(TMTSF)_2PF_6$. The spectrum of relaxation times $P_{t_w}(\log_{10} t)$ obtained from equation (2) is shown in Figure 1 for equilibrium relaxation and in Figure 2 for out-of-equilibrium relaxation. In both cases the long time tail of the spectrum of relaxation times is well described by a power-law. A similar power-law spectrum is obtained for the incommensurate SDW compound AsF_6 (see Fig. 3) and the incommensurate CDW compound TaS_3 (see Figs. 4 and 5).

It is visible on $(TMTSF)_2PF_6$ (see Fig. 2) and TaS_3 (see Fig. 5) that the exponent of the power-law relaxation

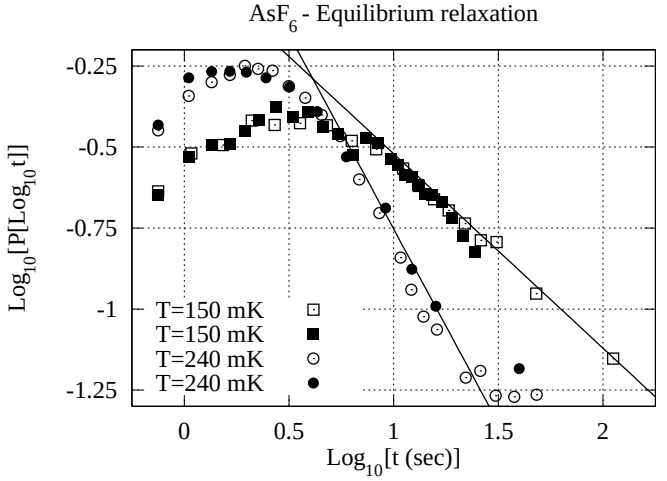

Fig. 3. Equilibrium relaxation time spectrum of the incommensurate SDW compound AsF_6 (a) for $T = 150$ mK and $t_w = 10$ min (□), $t_w = 1$ h (■); (b) for $T = 240$ mK and $t_w = 10$ min (○), $t_w = 1$ h (●). Equation (2) has been used to obtain the spectrum of relaxation times from the temperature relaxation signal. The long-time tail of the spectrum is well fitted by a power-law: $P_{\rm eq}(\log_{10} t) = 1.2 \times t^{-0.6}$ for $T = 150$ mK; $P_{\rm eq}(\log_{10} t) = 2.8 \times t^{-1.2}$ for $T = 240$ mK.

in the out-of-equilibrium dynamics is independent on the waiting time. The effect of the maximal relation time is also visible in Figure 5 where the long time relaxation is faster once equilibrium has been reached.

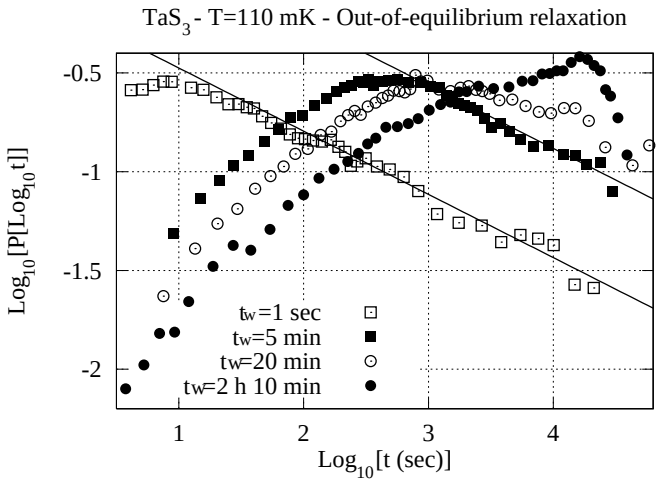

Fig. 4. Out-of-equilibrium relaxation time spectrum of the incommensurate CDW compound TaS_3 at the temperature $T = 110$ mK. Equation (2) has been used to obtain the spectrum of relaxation times from the temperature relaxation signal. The long-time tail of the spectrum is well fitted by a power-law: $P_{t_w}(\log_{10} t) = 0.7 \times t^{-0.32}$ for $t_w = 1$ sec; $P_{t_w}(\log_{10} t) = 2.5 \times t^{-0.32}$ for $t_w = 5$ min.

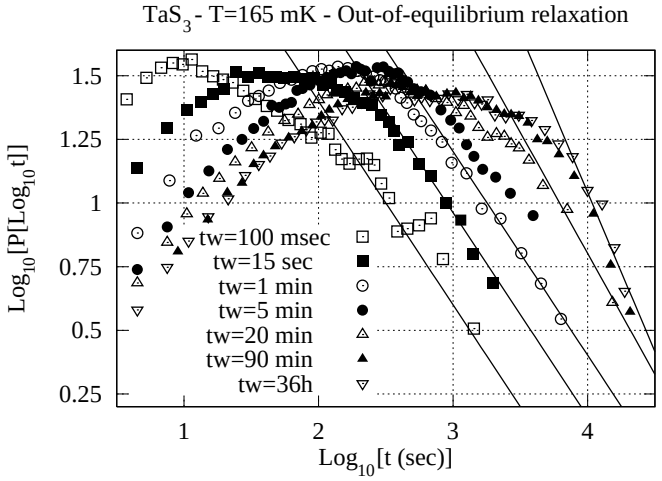

Fig. 5. Out-of-equilibrium relaxation time spectrum of the incommensurate CDW compound TaS_3 at the temperature $T = 165$ mK. Equation (2) has been used to obtain the spectrum of relaxation times from the temperature relaxation signal. The long-time tail of the spectrum is well fitted by a power-law: $P_{t_w}(\log_{10} t) = 10^3 \times t^{-0.8}$ for $t_w = 100$ msec; $P_{t_w}(\log_{10} t) = 2.3 \times 10^3 \times t^{-0.8}$ for $t_w = 15$ sec; $P_{t_w}(\log_{10} t) = 4 \times 10^3 \times t^{-0.8}$ for $t_w = 1$ min; $P_{t_w}(\log_{10} t) = 4 \times 10^4 \times t^{-0.95}$ for $t_w = 20$ min; $P_{t_w}(\log_{10} t) = 11 \times 10^5 \times t^{-1.25}$ for $t_w = 90$ min and $t_w = 36$ h.

3 Random energy-like trap models of disordered CDWs

We want to describe the slow relaxation experiments in CDWs and SDWs discussed in Section 2 by a REM-like trap model similar to references [49,57] (see Fig. 6). The "trap" energies $-E_\alpha$ are independent random variables chosen in a distribution $p(E_\alpha)$. The model with $p(E_\alpha) = p_0(E_\alpha) = 1/T_g \exp(-E_\alpha/T_g)$ solved by Bouchaud and Dean in reference [49] is recalled in Appendix A. We consider here a trap energy distribution in which there is a maximal energy barrier $E_{\max}$:

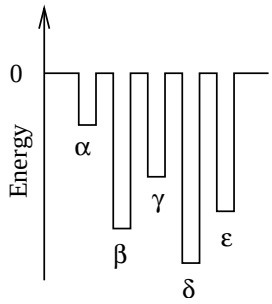

Fig. 6. Schematic representation of the phase space of a trap model. There are no traps having an energy barrier larger than $E_{\max}$. The maximum relaxation time is defined as $\tau_{\max} = \tau_0 \exp(E_{\max}/T)$.

$$p_1(E_\alpha) = \frac{1}{T_g} \frac{\exp(-E_\alpha/T_g)}{1 - \exp(-E_{\max}/T_g)} \text{ with } 0 < E_\alpha < E_{\max}. \tag{3}$$

The model with the trap distribution (3) has two properties related to the experiments discussed in Section 2:

(i) "Interrupted ageing" behavior due to the presence of a maximal energy barrier. The "complexity" $\Omega = (T/T_g) \ln(\tau_{\rm erg}/\tau_0)$ introduced in reference [49] is equal to $\Omega = E_{\max}/T_g$.

(ii) A power-law distribution of relaxation times for $\tau_\alpha < \tau_{\max}$:

$$p_1(\tau_\alpha) = \frac{1}{\tau_0} \frac{T}{T_g} \frac{1}{1 - \exp(-E_{\max})} \left(\frac{\tau_0}{\tau_\alpha}\right)^{1+T/T_g}. \tag{4}$$

3.1 Average and typical relaxation times

The average relaxation time is defined by $\tau_{\rm av} = \int \tau P(\log_{10}\tau) {\rm d}\log_{10}\tau$. For the model with the trap energy distribution (3) we find

$$\frac{\tau^{\rm av}}{\tau^0} = \frac{T}{T - T_g} \frac{1 - \exp[-(1 - T_g/T)(E_{\max}/T_g)]}{1 - \exp(-(E_{\max}/T_g))}. \tag{5}$$

The typical relaxation time corresponds to the maximum of $P(\log_{10}\tau)$ and is defined as $\tau^{\rm typ} = \exp[\langle\langle \ln \tau_\alpha \rangle\rangle]$, where τ_α is the trapping time in trap α: $\tau_\alpha = \tau_0 \exp(E_\alpha/T)$. With the trap energy distribution (3) we find

$$\frac{\tau^{\rm typ}}{\tau^0} = \exp\left[\frac{T_g}{T}\left[1 - \frac{(E_{\max}/T_g)}{\exp(E_{\max}/T_g) - 1}\right]\right], \tag{6}$$

which reduces to $\tau^{\rm typ} \simeq \tau^0 \exp[T_g/T]$ if $E_{\max}$ is large compared to T_g. The activated behavior of the typical relaxation time is in agreement with previous experimental

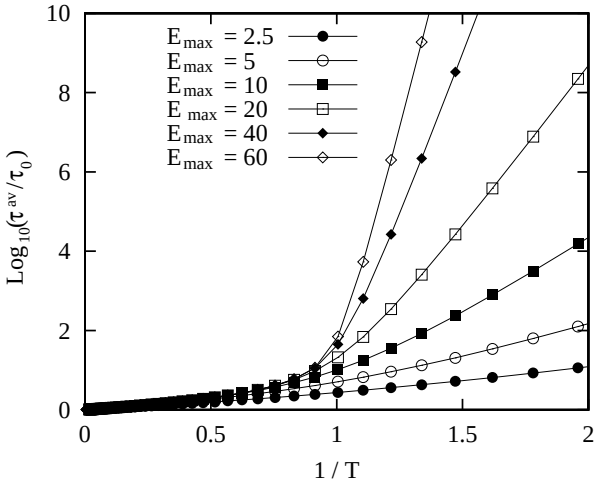

Fig. 7. Evolution of the logarithm of the average relaxation time $\log_{10}(\tau^{\rm av}/\tau_0)$ *versus* $1/T$ with $T_g = 1$ and different values of $E_{\rm max}$.

observations [48]. The variation of the average relaxation time *versus* $1/T$ is shown in Figure 7. If $E_{\rm max}$ is weak there is an activated behavior for all values of the temperature, even below T_g. If $E_{\rm max}$ increases there is a strong slowing down of the dynamics below T_g and the average relaxation time is infinite when $E_{\rm max}$ is infinite in which case we recover the behavior considered in reference [49]. The average relaxation time plays a central role in the weak ergodicity breaking scenario for spin-glass models (see Appendix A) but does not play a relevant role in slow relaxation in CDWs and SDWs because it cannot be deduced from experiments in these systems.

3.2 Relaxation below the glass cross-over temperature T_g

We use the approximations presented in Appendix A.2 to evaluate the dynamical correlation function $\Pi_1(t,t_w)$ associated to the model having a maximal energy barrier $E_{\rm max}$:

$$\Pi_1(t,t_w) \simeq \left[1-\left(\frac{T}{T_g}\right)^2\right]\left(\frac{t_w}{t}\right)^{T/T_g} \quad \text{if } t_w \ll t \ll \tau_{\rm max} \tag{7}$$

$$\Pi_1(t,t_w) \simeq 1-\left(\frac{T}{T_g}\right)^2\left(\frac{t}{t_w}\right)^{1-T/T_g} \quad \text{if } t \ll t_w \ll \tau_{\rm max} \tag{8}$$

$$\Pi_1(t,t_w) \simeq 1 \text{ if } t \ll \tau_{\rm max} \ll t_w. \tag{9}$$

We make two comments:

(i) The system has thermalized before t_w if $t_w \gg \tau_{\rm max}$. In this case, the correlation function decays exponentially with time: $\Pi(t,t_w) \sim \exp(-t/\tau_{\rm max})$. Within the approximation used here, this corresponds to $\Pi(t,t_w) \simeq 1$ if $t \ll \tau_{\rm max}$ and $\Pi(t,t_w) \simeq 0$ if $t \gg \tau_{\rm max}$.

Table 1. Values of $\alpha_{\rm exp}$ corresponding to the experiments in Section 2. We have indicated the estimated values of T/T_g and the estimated value of the glass cross-over temperature T_g.

Compound	T (mK)	$\alpha_{\rm exp}$	T/T_g	T_g (mK)
$(TMTSF)_2PF_6$	200	0.4	1.4	142
$(TMTSF)_2PF_6$	400	0.5	1.5	267
$(TMTSF)_2PF_6$	500	0.7	1.7	294
AsF_6	150	0.6	1.6	94
AsF_6	240	1.2	2.2	109
TaS_3	110	0.3	1.3	83
TaS_3	165	0.8	1.8	92

(ii) If $t, t_w \ll \tau_{\rm max}$, the system has no time to "experience" the existence of the maximal energy barrier $E_{\rm max}$. The out-of-equilibrium relaxation is identical to the model discussed in Appendix A.

3.3 Relaxation above the glass cross-over temperature T_g

Relaxation above the glass cross-over temperature is directly relevant to experiments. Above the glass cross-over temperature the correlation function deduced from the approximations in Appendix A are found to be

$$\Pi_1(t,t_w) \simeq 2\left(1-\frac{T_g}{T}\right)\left(\frac{\tau_0}{t}\right)^{T/T_g}\frac{t_w}{\tau_0} \quad \text{if } t_w \ll t \ll \tau_{\rm max} \tag{10}$$

$$\Pi_1(t,t_w) \simeq \left(\frac{\tau_0}{t}\right)^{T/T_g-1} \quad \text{if } t \ll t_w \ll \tau_{\rm max} \tag{11}$$

$$\Pi_1(t,t_w) \simeq \left(\frac{\tau_0}{t}\right)^{T/T_g-1} \quad \text{if } t \ll \tau_{\rm max} \ll t_w. \tag{12}$$

The spectrum of relaxation times is a power-law if $t \ll t_w \ll \tau_{\rm max}$: $\partial\Pi_1/\partial \ln t \sim t^{1-T/T_g}$. The exponent $1-T/T_g$ does not depend on t_w. This coincides with the experimental behavior discussed in Section 2 (see Figs. 2 and 4). The model can be used to deduce an estimate of the glass cross-over temperature T_g from the exponents obtained in experiments (see Sect. 2). T_g is related to the exponent $\alpha_{\rm exp}$ appearing in the experimental power-law relaxation spectrum $P_{t_w}(\log_{10} t) \sim t^{-\alpha_{\rm exp}}$ through the relation $T/T_g = 1+\alpha_{\rm exp}$. The values of $\alpha_{\rm exp}$ and the estimations of T_g deduced from the correspondence between the experiments and the REM-like trap model have been given on Table 1. For the three compounds $(TMTSF)_2PF_6$, AsF_6 and TaS_3, the exponent $\alpha_{\rm exp}$ is increasing with temperature which constitutes a qualitative agreement between experiments and the REM-like trap model. The values of T_g are of the order of $T_g = 100 \div 200$ mK. We should note that the model cannot be used to describe heat pulse relaxation in the regime $t \gg t_w$. Namely Figure 2 and Figure 5 suggest that the exponent $\alpha_{\rm exp}$ is the same if $t \ll t_w$ or $t_w \ll t$ while equations (10–12) would predict a different power-law in the regimes $t \ll t_w$ and $t_w \ll t$. This is an indication that the exponential trap distribution with a cut-off is not well suited to describe the short time dynamics.

4 Collective dynamics in a strong pinning model

4.1 The model

Let us now consider the microscopic model discussed by several authors in references [52–56] that is used to describe the pinning of a disordered CDW:

$$\mathcal{H} = \frac{v_F}{4\pi}\int \mathrm{d}x \left(\frac{\partial\varphi(x)}{\partial x}\right)^2 + w\int \mathrm{d}x\,[1-\cos\varphi(x)] - \sum_i V_i\,[1-\cos\left(Qx_i+\varphi(x_i)\right)]. \quad (13)$$

The first term in equation (13) is the elastic energy, the second term is the interchain interaction, and the third term is the pining potential. The charge density wave vector is Q and the impurities are at random positions x_i along the chain.

4.2 One strong pinning impurity

Let us recall the solution of the one-impurity model discussed in references [55,56]. With $V_i = 0$, $\varphi(x)$ is the solution of the sine Gordon-like equation

$$w\sin\varphi(x) - \frac{v_F}{2\pi}\frac{\partial^2\varphi(x)}{\partial x^2} - V\delta(x-x_1)\sin\varphi(x) = 0. \quad (14)$$

The low-energy solutions are dipoles made of a superposition of two solitons:

$$\tan\left(\frac{\varphi(x)}{4}\right) = \tan\left(\frac{\psi}{4}\right)\exp\left(-\frac{|x-x_1|}{\xi_0}\right). \quad (15)$$

The width of the soliton is

$$\xi_0 = \sqrt{\frac{v_F}{2\pi w}}\,. \quad (16)$$

For commensurate impurities having $Qx_1 = 0$, ψ is the solution of $\cos(\psi/2) = V_c^{(1)}/V$, where the one-impurity pinning threshold is given by $V_c^{(1)} = \sqrt{2wv_F/\pi}$. With $V > V_c^{(1)}$ there is one unstable solution ($\psi = 0$) and there are two stable solutions $\psi = \pm 2\arccos(V_c^{(1)}/V)$. The single impurity solutions are degenerate and their total energy is $E_{\mathrm{tot}}^{(1)} = -2(V - V_c^{(1)})^2/V$. With incommensurate impurities ($Qx_1 \neq 0$), ψ is the solution of

$$\frac{2v_F}{\pi\xi_0}\sin\left(\frac{\psi}{2}\right) = V\sin\left(Qx_1+\psi\right). \quad (17)$$

The dipolar low-energy excitations were discussed in reference [56] for independent impurities close to commensurability ($Qx_1 \ll 1$). Equation (17) can be solved numerically if Qx_1 is not a small parameter.

Another way of solving the one-impurity model is to consider the soliton profile given by (15) as a variational solution parametrized by ψ. The energy landscape associated to a single impurity is the following:

$$E_{\mathrm{tot}}^{(1)}(X_0) = -\frac{1}{(1+X_0^2)^2}\left\{A(x_1) + B(x_1)X_0 - (16w\xi_0 - C(x_1))\,X_0^2 - B(x_1)X_0^3 - (16w\xi_0 - A(x_1))\,X_0^4\right\}, \quad (18)$$

where $X_0 = \tan(\psi/4)$. The coefficients $A(x_1)$, $B(x_1)$ and $C(x_1)$ are given by

$$A(x_1) = 2V\sin^2(Qx_1) \quad (19)$$

$$B(x_1) = 4V\sin(Qx_1) \quad (20)$$

$$C(x_1) = 2V\,[1+3\cos(Qx_1)]. \quad (21)$$

Minimizing equation (18) with respect to X_0 leads directly to equation (17). For commensurate impurities there are two degenerate energy minima separated by an energy barrier. For incommensurate impurities the two energy minima are not degenerate (there is a metastable state).

4.3 Two strong pinning impurities

The purpose of this section is to replace a cluster made of two impurities by a single effective impurity. We start with the case of two impurities that are close to each other ($|x_2 - x_1| \ll \xi_0$). The opposite limit $|x_2 - x_1| \gg \xi_0$ is discussed in a straightforward fashion because in this case the two impurities have an independent dynamics. An approximate solution for an arbitrary $|x_2 - x_1|$ can be obtained by interpolating between the two limiting cases $|x_2 - x_1| \ll \xi_0$ and $|x_2 - x_1| \gg \xi_0$.

4.3.1 Variational soliton profile

We look for variational solutions describing two impurities at positions x_1 and $x_2 > x_1$ under the form $\tan(\varphi(x)/4) = F(x)$, with

$$F(x) = \tan\left(\frac{\psi_1}{4}\right)\exp\left(-\frac{|x-x_1|}{\xi_0}\right) + \tan\left(\frac{\psi_2}{4}\right)\exp\left(-\frac{|x-x_2|}{\xi_0}\right), \quad (22)$$

where ψ_1 and ψ_2 are variational parameters that can be determined by minimizing the total energy obtained from the soliton profile (22). If the distance between the two impurities is much smaller than ξ_0 ($|x_2 - x_1| \ll \xi_0$) the two-impurity energy landscape $E_{\mathrm{tot}}^{(2)}(X_0)$ is a function of the single parameter X_0 given by

$$X_0 = \tan\left(\frac{\psi_1}{4}\right) + \tan\left(\frac{\psi_2}{4}\right). \quad (23)$$

4.3.2 Commensurate impurities in the limit $|x_2 - x_1| \ll \xi_0$

Let us now consider the situation where the two impurities at positions x_1 and x_2 are commensurate and the distance between the two impurities is small compared to the width of the soliton ($|x_2 - x_1| \ll \xi_0$). The total energy of the two-impurity system takes the form

$$E_{\rm tot}^{(2)}(X_0) = \frac{16X_0^2}{(1+X_0^2)^2}\left\{w\xi_0 - V + w\xi_0 X_0^2\right\}.$$

The ground state is such that $\partial E_{\rm tot}^{(2)}(X_0^*)/\partial X_0 = 0$, which leads to

$$X_0^* = \sqrt{\frac{V - w\xi_0}{V + w\xi_0}} \tag{24}$$

$$E_{\rm tot}^{(2)}(X_0^*) = -\frac{4}{V}\left(V - w\xi_0\right)^2. \tag{25}$$

We make two remarks:

(i) The pinning threshold associated to two commensurate impurities such that $|x_2 - x_1| \ll \xi_0$ is $V_c^{(2)} = w\xi_0 = 2V_c^{(1)}$, equal to two times the pinning threshold associated to a single impurity. The interaction between impurities increases the pinning threshold and favors the so-called "collective pinning" regime corresponding to $V < V_c^{(2)}$, as opposed to the "strong pinning" regime corresponding to $V > V_c^{(2)}$.

(ii) In the limit of strong impurity pinning ($V \gg w\xi_0$), there are two energy minima corresponding to $X_0 = \tan(\psi/4) + \tan(\psi'/4) = \pm 1$ and having an energy $E_{\rm tot}^{(2)}(X_0^*) = -4V$. These two minima are separated by the saddle point $X_0' = \tan(\psi/4) + \tan(\psi'/4) = 0$ having an energy $E_{\rm tot}^{(2)}(X_0') = 0$. If $V \gg w\xi_0$ and $|x_2 - x_1| \ll \xi_0$, the energy barrier associated to the two impurity system is $\Delta E^{(2)} = E_{\rm tot}(X_0') - E_{\rm tot}(X_0) = 4V$, equal to two times the energy barrier associated to a single impurity: $\Delta E^{(1)} = 2V$ (see Sect. 4.2). This shows that the interaction between impurities makes the system more glassy.

4.3.3 Incommensurate impurities in the limit $|x_2 - x_1| \ll \xi_0$

The energy landscape associated to two incommensurate impurities at a distance much smaller than the soliton width ($|x_2 - x_1| \ll \xi_0$) can be reduced to an effective single impurity energy landscape:

$$E_{\rm tot}^{(2)}(X_0) = -\frac{1}{(1+X_0^2)^2}\left\{\tilde{A}_0 + \tilde{B}_0 X_0 - \left(16w\xi_0 - \tilde{C}_0\right)X_0^2 - \tilde{B}_0 X_0^3 - \left(16w\xi_0 - \tilde{A}_0\right)X_0^4\right\}. \tag{26}$$

The coefficients $\tilde{A}_0$, $\tilde{B}_0$ and $\tilde{C}_0$ are obtained as the sum of the coefficients associated to the single impurity energy landscapes given by equations (19–21): $\tilde{A}_0 = A(x_1) + A(x_2)$, $\tilde{B}_0 = B(x_1) + B(x_2)$, and $\tilde{B}_0 = C(x_1) + C(x_2)$. The form (26) of the two-impurity energy landscape can be understood as follows. The elastic and interchain energy of the two-impurity model are identical to the one-impurity model if one uses the variables $X_0 = \tan(\psi/4)$ for the one-impurity system and $X_0 = \tan(\psi/4) + \tan(\psi'/4)$ for the two-impurity system. The pinning energy is additive since the phase of the CDW at x_1 is approximately equal to the phase of the CDW at x_2 if $|x_2 - x_1| \ll \xi_0$.

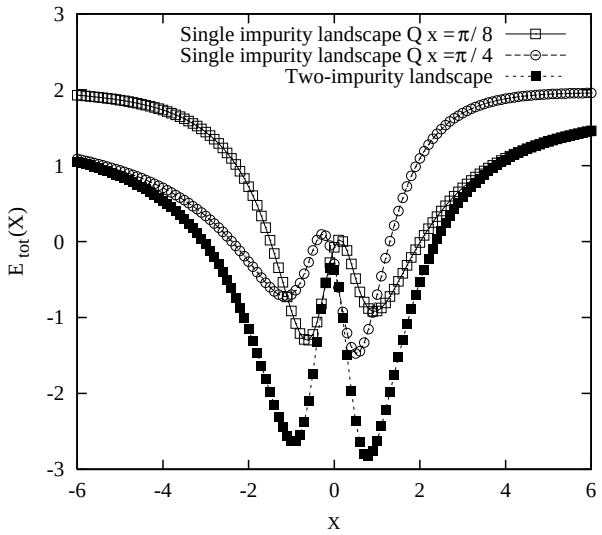

Fig. 8. Energy landscape $E_{\rm tot}^{(1)}(X)$ *versus* X given by Equation (18) of two isolated impurities being far apart and such that $Qx_1 = \pi/8$ (○) and $Qx_2 = \pi/4$ (□). If these two impurities are at a distance much smaller than ξ_0 the two-impurity system can be represented by an effective impurity having an energy landscape $E_{\rm tot}^{(2)}(X)$ (see Eq. (26)). The energy landscape $E_{\rm tot}^{(2)}(X)$ is also shown on the figure (■).

4.3.4 Limit $|x_1 - x_2| \gg \xi_0$

If the two impurities are at a distance much larger than the soliton width ($|x_2 - x_1| \gg \xi_0$) the two impurities have an independent dynamics. The two impurities are characterized by the coefficients (A_1, B_1, C_1) and (A_2, B_2, C_2) (see Eq. (18)). The two decoupled impurities can be replaced by a single impurity characterized by the coefficients $(\tilde{A}_\infty, \tilde{B}_\infty, \tilde{C}_\infty)$. The coefficients $(\tilde{A}_\infty, \tilde{B}_\infty, \tilde{C}_\infty)$ correspond either to (A_1, B_1, C_1) if the impurity at position x_1 has the longest relaxation time or to (A_2, B_2, C_2) if the impurity at position x_2 has the longest relaxation time.

4.3.5 Interpolation between the limits $|x_2 - x_1| \ll \xi_0$ and $|x_2 - x_1| \gg \xi_0$

An arbitrary value of the distance between the impurities can be treated by interpolating between the two limiting cases $|x_2 - x_1| \ll \xi_0$ and $|x_2 - x_1| \gg \xi_0$ discussed above.

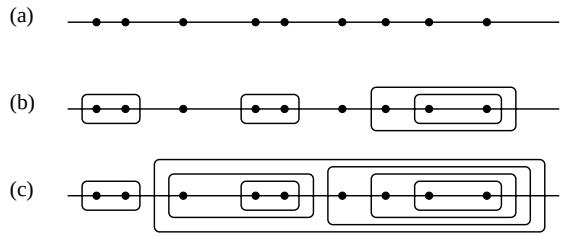

Fig. 9. Schematic representation of the formation of correlated objects in the collective dynamics. (a) corresponds to decoupled impurities (which is the initial condition of the RG flow at time t_0). (b) corresponds to a time $t_1 > t_0$. (c) corresponds to a time $t_2 > t_1 > t_0$. The correlation length is increasing with time: $\xi(t_2) > \xi(t_1) > \xi(t_0)$.

Namely we suppose that the energy landscape at an arbitrary distance $|x_2 - x_1|$ is still given by equation (26):

$$E^{(2)}_{\rm tot}(X_0) = -\frac{1}{(1+X_0^2)^2}\left\{\tilde{A} + \tilde{B}X_0 - \left(16w\xi_0 - \tilde{C}\right)X_0^2 - \tilde{B}X_0^3 - \left(16w\xi_0 - \tilde{A}\right)X_0^4\right\}, \quad (27)$$

and that the coefficients $\tilde{A}$, $\tilde{B}$ and $\tilde{C}$ interpolate between the solutions already obtained in the limits $|x_2 - x_1| \ll \xi_0$ and $|x_2 - x_1| \gg \xi_0$:

$$\tilde{A} = \tilde{A}_\infty + \left(\tilde{A}_0 - \tilde{A}_\infty\right)\exp\left(-\frac{|x_2 - x_1|}{\xi_0}\right) \quad (28)$$

$$\tilde{B} = \tilde{B}_\infty + \left(\tilde{B}_0 - \tilde{B}_\infty\right)\exp\left(-\frac{|x_2 - x_1|}{\xi_0}\right) \quad (29)$$

$$\tilde{C} = \tilde{C}_\infty + \left(\tilde{C}_0 - \tilde{C}_\infty\right)\exp\left(-\frac{|x_2 - x_1|}{\xi_0}\right). \quad (30)$$

The correlations mediated by the gaped medium decay exponentially with distance and this is why we use an exponential interpolation in equations (28–30).

4.4 Dynamical RG

Now we discuss the collective dynamics of the model defined by equation (13). The method is similar to reference [10] and consists in eliminating the fastest degrees of freedom (see Fig. 9). There is a smallest relaxation time $\tau_{\rm min}$ (being the smallest of the relaxation times of individual impurities) that increases in the course of the RG. Assuming a broad distribution of relaxation times, the density of relaxation times is given by the number of impurities $\rho(\tau_{\rm min})\delta\tau_{\rm mnin}$ that are eliminated as the smallest relaxation time is increased from $\tau_{\rm min}$ to $\tau_{\rm min} + \delta\tau_{\rm min}$.

We consider that the initial condition of the dynamics is a quench from high temperature. The initial condition of the RG flow corresponds to uncorrelated impurities. The experiments discussed in Section 2 correspond to a different initial condition but it is expected that the two types of initial conditions can be used to discuss the qualitative physics.

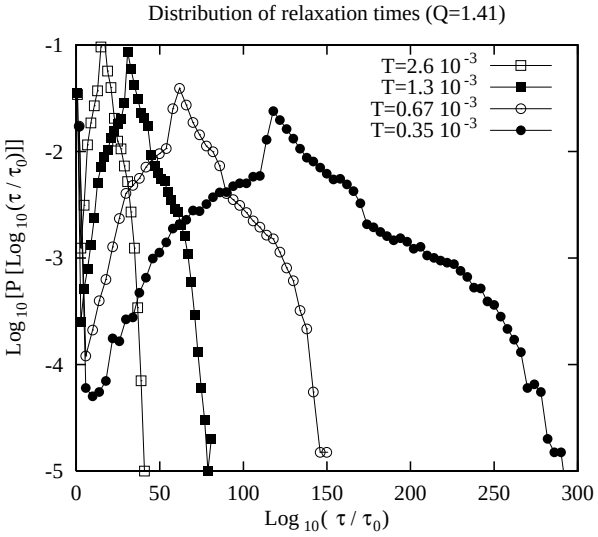

Fig. 10. Distribution of the logarithm of the relaxation times with an incommensurate CDW wave vector ($Q = \sqrt{2} \simeq 1.41$). The distribution of relaxation times has been obtained with $N = 500$ impurities and averaged over 100 realizations of disorder. The parameters of the strong pinning Hamiltonian given by equation (13) are $v_F = 1$, $w = 5 \times 10^{-6}$, $V_i = 56 \times 10^{-3}$ for all sites i. The correlation length in the simulation is $\xi = 178a_0$, with a_0 the lattice spacing. The one-impurity pinning threshold is $V_c = 5.6 \times 10^{-3}$. The impurity concentration is $x = 0.05 \ll 1$. The temperature in units of v_F corresponding to the different curves are: $T = 2.6 \times 10^{-3}$ (□), $T = 1.3 \times 10^{-3}$ (■), $T = 0.67 \times 10^{-3}$ (○), $T = 0.35 \times 10^{-3}$ (●). The parameters are such that the width of the soliton ξ and the ratio T/v_F have the correct order of magnitude. For instance $\xi \simeq 4000$ Å in CDW compounds and $a_0 \simeq 3 \div 7$ Å ($a_0 = 3.34$ Å in TaS_3 and $a_0 = 7.3$ Å in $(TMTSF)_2PF_6$). We deduce that $\xi \simeq 500 \div 1000a_0$ which is compatible with the value of ξ used in the simulation. The value of the impurity concentration x is also realistic in the sense that it has been shown experimentally that the introduction of 0.5% of extrinsic impurities does not modify the slow relaxation properties so that x is presumably larger than 0.5%.

The energy landscape of an impurity at site x_i is characterized by the coefficients $(A(x_i), B(x_i), C(x_i))$ (see Eq. (18)) and by a relaxation time τ_i. We note by $\tau_{\rm min} = {\rm Min}\{\tau_i\}$ the smallest of these relaxation times corresponding to impurity i_0. The impurity i_0 has two neighboring impurities: one at the left (site i_L) and one at the right (site i_R). The relaxation times of the impurities at sites i_L and i_R are τ_L and τ_R. There are two possibilities to eliminate the impurity at site i_0:

(i) Transform the two impurities at sites i_0 and i_L into an effective impurity at site i'_L having a relaxation time τ'_L.
(ii) Transform the two impurities at sites i_0 and i_R into an effective impurity at site i'_R having a relaxation time τ'_R.

The transformation (i) is implemented if $\tau'_L < \tau'_R$. The transformation (ii) is implemented if $\tau'_R < \tau'_L$.

The distribution of relaxation times is shown in Figure 10 for an incommensurate CDW wave vector and in

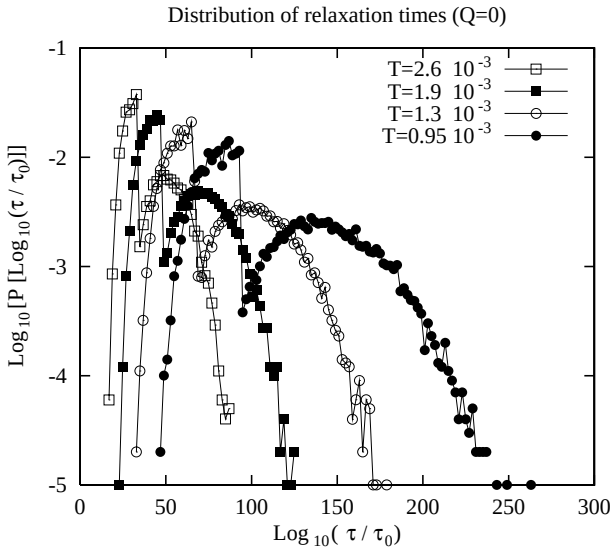

Fig. 11. Distribution of the relaxation times in the presence of commensurate impurities having $Q = 0$. The Hamiltonian parameters are identical to Figure 10. The temperature in units of v_F are: $T = 2.6 \times 10^{-3}$ (□), $T = 1.9 \times 10^{-3}$ (■), $T = 1.3 \times 10^{-3}$ (○), $T = 0.95 \times 10^{-3}$ (●).

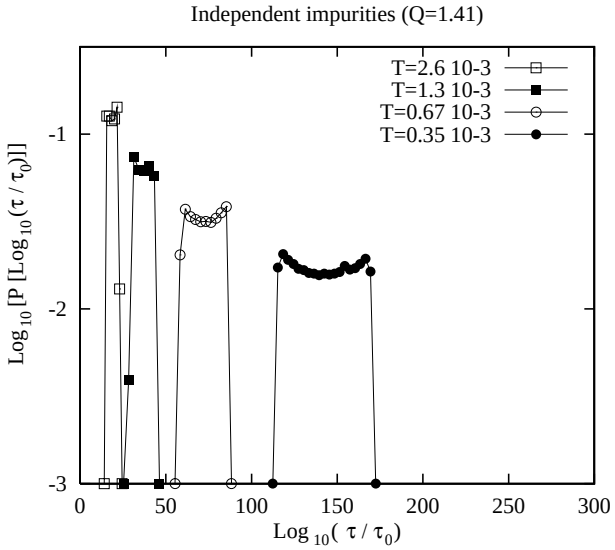

Fig. 12. The same as Figure 10 but with non interacting impurities (this is the initial condition of the RG flow).

Figure 11 for a commensurate CDW wave vector. The two systems are qualitatively similar in the sense that (i) the collective dynamics generates a broad spectrum of relaxation times; and (ii) there is a maximum relaxation time $\tau_{\max}$. At long times, the spectrum of relaxation times is approximately a power-law, which is not against the experiments discussed in Section 2. For comparison we have shown in Figure 12 the distribution of relaxation times of non interacting strong pinning impurities with the same parameters as Figure 10. There is already a distribution of relaxation times associated to independent impurities which is due to the fact that the energy landscape associated to an impurity at position x_1 depends on the coordinate x_1 through equations (19–21). But the distribution of relaxation times of interacting impurities is obviously much broader than the distribution of relaxation times of non interacting impurities (see Figs. 10 and 12). Given that there are evidences that a broad spectrum of relaxation times is present in the slow relaxation experiments either for commensurate of incommensurate systems, we conclude that the long time dynamics of disordered CDWs and SDWs is a collective phenomenon that can be qualitatively captured by the dynamical RG of the strong pinning model. The small time dynamics can be well approximated by independent impurities corresponding to Figure 12 on the condition that the initial condition is a quench from high temperature.

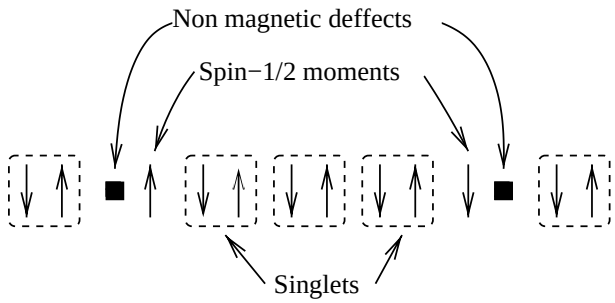

Fig. 13. Schematic representation of non magnetic substitutions in a spin-Peierls system. We assume that the spin-1/2 solitonic moments have a slow dynamics.

5 Collective dynamics in a disordered spin-Peierls system

5.1 The model

Now we consider the model introduced in references [30,44,45] to describe non magnetic substitutions in spin-Peierls and Haldane gap systems (see Fig. 13). In this model non magnetic impurities in a dimerized system generate solitonic spin-1/2 moments out of the non magnetic singlets. Two spin-1/2 moments at distance l are coupled by an antiferromagnetic exchange $J(l) = \Delta \exp(-l/\xi_0)$ that decays exponentially with distance. ξ_0 is the correlation length associated to the gaped background. There is an energy barrier associated to the dynamics of an isolated soliton in CDWs and SDWs (see for instance Fig. 8) which explains that the microscopic time τ_0 is of order of 1 sec (see [46–48]). The model proposed for non magnetic substitutions in $CuGeO_3$ can thus be "transformed" into a model of slow relaxation in CDWs and SDWs just by changing the time scale τ_0 associated to the dynamics of individual solitonic spin-1/2 moments. From this analogy we deduce an expression of the glass cross-over temperature of disordered CDWs and SDWs.

We represent the solitonic spin-1/2 degrees of freedom in the spin-Peierls system by Ising spins distributed at random in 1D (see Fig. 14) and use a Glauber dynamics.

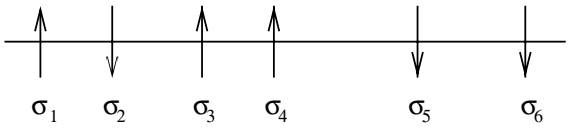

Fig. 14. Schematic representation of the Ising model. The spins σ_i are distributed at random in 1D and interact with the Hamiltonian (31).

The Ising spins σ_i interact with the Hamiltonian

$$\mathcal{H} = -\sum_{\langle i,j \rangle} J_{i,j}\sigma_i\sigma_j, \tag{31}$$

where the exchange $J_{i,j}$ decays exponentially with distance (see Refs. [44,45]):

$$J_{i,j} = \Delta \exp\left(-\frac{d_{i,j}}{\xi_0}\right). \tag{32}$$

Δ is the spin gap, ξ_0 is the correlation length associated to the CDW without disorder (see Eq. (16) for the expression of ξ_0 in the strong pinning model), and $d_{i,j}$ is the distance between the Ising spins at sites i and j. Since there is no frustration the dynamics of the ferromagnetic and antiferromagnetic models are equivalent and we use here the ferromagnetic model. The single spin flip Glauber dynamics of the model defined by equations (31) and (32) is given by the master equation [58]

$$\frac{\mathrm{d}}{\mathrm{d}t}P(\{\sigma\},t) = -\sum_{i=1}^{N} w_i\{\sigma\}P(\{\sigma\},t) + \sum_{i=1}^{N} w_i\{\sigma_1,...,-\check{\sigma}_i,...,\sigma_N\}P(\{\sigma_1,...,-\check{\sigma}_i,...,\sigma_N\},t), \tag{33}$$

where the transition rates take the form

$$w_i\{\sigma\} = \frac{r_i}{2}\left(1 - \sigma_i \tanh\left(\beta J_{i,j}\sum_{j\in V(i)}\sigma_j\right)\right), \tag{34}$$

where $V(i)$ is the set of neighbors of site i. The form of the transition rates given by equation (34) ensures that the detailed balance is verified: $P_B\{\sigma\}w_i\{\sigma\} = P_B\{\sigma'\}w_i\{\sigma_1,...,-\check{\sigma}_i,...,\sigma\}$, where $P_B\{\sigma\}$ is the Boltzmann distribution.

5.2 Two-spin model

Following references [30,44,45] we consider the model defined by equations (31) and (32) for two Ising spins σ_1 and σ_2 at distance l. The distribution of distances is $P(l) = x\exp(-xl)$ and the exchange (32) becomes $J(l) = \Delta\exp(-l/\xi_0)$. The relaxation time associated to the two-spin cluster can be obtained from the Glauber matrix defined by (33): $\tau(l) = \tau_0\left[1 - \tanh\left(J(l)/T\right)\right]^{-1}$. Since we consider the long-time behavior, we use the approximation $\tau(l) \simeq \frac{\tau_0}{2}\exp\left[2J(l)/T\right]$. The typical relaxation time follows an Aharenius behavior:

$$\frac{\tau^{\mathrm{typ}}}{\tau_0} = \exp\left(\langle\langle \ln\left(\frac{\tau(l)}{\tau_0}\right)\rangle\rangle\right) = \frac{1}{2}\exp\left(\frac{2x\xi_0}{1+x\xi_0}\frac{\Delta}{T}\right). \tag{35}$$

The activation energy in equation (35) is equal to the average energy barrier given by $2\langle\langle J(l)\rangle\rangle = 2x\xi_0/(1+x\xi_0)$. The average relaxation time is given by an Aharenius law in limit of a small dilution of impurities ($x\xi_0 \ll 1$):

$$\frac{\tau^{\mathrm{av}}}{\tau_0} = \langle\langle\frac{\tau(l)}{\tau_0}\rangle\rangle \simeq \frac{1}{4}\frac{x\xi_0 T}{\Delta}\exp\left(\frac{2\Delta}{T}\right). \tag{36}$$

The activation energy in equation (36) is equal to the largest energy barrier given by $2\mathrm{Max}[J(l)] = 2\Delta$.

Comparing the typical relaxation time in the REM-like model and the two-spin model (see Eqs. (5) and (36)) we obtain an estimate of the glass cross-over temperature in terms of the microscopic parameters:

$$T_g = \frac{2x\xi_0\Delta}{1+x\xi_0} \tag{37}$$

which is equal to the average energy barrier. The estimate of T_g given by equation (37) is similar to the estimate of the Néel temperature of doped low dimensional oxides discussed in references [44,45]. In both cases the physics is controlled by correlations among the solitons.

5.3 RG of the disordered 1D Ising model

Let us consider two Ising spins σ_1 and σ_2 coupled by a ferromagnetic exchange J and replace these two spins by an effective Ising spin $\tilde{\sigma}$. We note τ_1 and τ_2 the relaxation times of the spins σ_1 and σ_2 and we note $r_1 = 1/\tau_1$ and $r_2 = 1/\tau_2$ the transition rates. The Glauber matrix of the two-spin system can be diagonalized by forming symmetric and antisymmetric combinations of the occupation probabilities [61]. We deduce the transition rate $\tilde{r}$ of the effective spin $\tilde{\sigma}$:

$$\tilde{r} = \frac{1}{2}\left\{r_1 + r_2 - \sqrt{(r_1-r_2)^2 + 4r_1r_2\tanh^2(\beta J)}\right\}. \tag{38}$$

The couplings $\tilde{J}_L$ and $\tilde{J}_R$ between the effective spin $\tilde{\sigma}$ and its neighboring spins (see Fig. 15) can be obtained by equating the partition function of the four-spin system and the partition function of the three-spin system, leading to

$$\tilde{J}_R = T\,\mathrm{arg\,cosh}\left[\sqrt{2}\sqrt{\cosh(\beta J)}\cosh(\beta J_R)\right] \tag{39}$$

$$\tilde{J}_L = T\,\mathrm{arg\,cosh}\left[\sqrt{2}\sqrt{\cosh(\beta J)}\cosh(\beta J_L)\right]. \tag{40}$$

The RG transformations can be iterated by eliminating the smallest relaxation time $\tau_{\min} = \mathrm{Min}\{\tau_i^{(1)}, \tau_{i,i+1}^{(2)}\}$

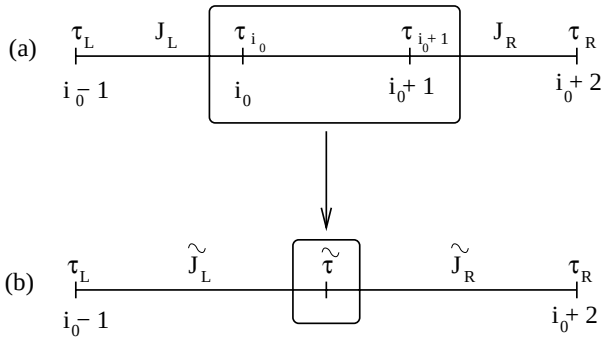

Fig. 15. Representation of the RG transformation. The pair of spins $(\sigma_{i_0}, \sigma_{i_0+1})$ is replaced by the effective Ising spin $\tilde{\sigma}$ having a relaxation rate $\tilde{r} = 1/\tilde{\tau}$ given by equation (38).

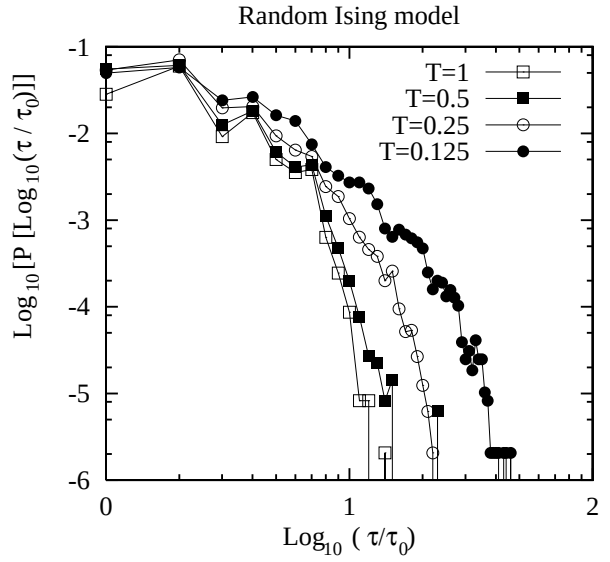

Fig. 16. Distribution of the logarithm of the relaxation times of the random Ising model defined by (31) and (32) with the parameters $\Delta = 1$, $\xi = 10$, and $x = 0.05$, with four different temperatures: $T = 1$ (□), $T = 0.5$ (■), $T = 0.25$ (○) and $T = 0.125$ (●). The "microscopic" time scale is $\tau_0 = 1$.

which is either the relaxation time $\tau_i^{(1)}$ associated to a single spin or the relaxation time $\tau_{i,i+1}^{(2)}$ associated to the pair of spins $(i, i+1)$.

The distribution of logarithm of the relaxation times is shown in Figure 16. Because of the collective dynamics there is a broad distribution of relaxation times and a maximum relaxation time $\tau_{\max}$, which is compatible with the experiments discussed in Section 2. The disordered spin-Peierls system discussed in this section has thus the same behavior as the disordered strong pinning model discussed in Section 4. In the case of the Ising model (see Fig. 16) the RG generates only time scales that are larger than τ_0. In the case of the disordered strong pinning model the RG generates time scales that are also smaller than τ_0 (being the relaxation time of individual solitons) which explains the origin of the maximum in the relaxation time spectrum (see Fig. 10).

6 Conclusion

To conclude we have discussed the collective dynamics of randomly distributed solitons and shown that this approach was relevant to disordered CDWs and SDWs. We have proposed a phenomenological REM-like model that in good agreement with experiments. Since the article was already summarized in the Introduction, we end-up with open questions:

(i) We assumed that the solitons are decoupled from each other in the initial condition of the RG. This corresponds to a quench from high temperature. The initial condition relevant to the experiments in Section 2 is different because the dynamics starts from an equilibrium state and a small temperature variation is applied. It has been pointed out that there can be a specific dynamics associated to the temperature dependence of the equilibrium correlation length [62] and it is thus a relevant question to examine similar issues in CDWs and SDWs.

(ii) We have assumed that only charge or spin degrees of freedom were relevant in CDWs or SDWs. The interplay between charge and spin degrees of freedom raises many questions already in pure systems (see for instance [63]). It is an open question to examine the physics associated to defects in the presence of a charge and a spin sector. The interplay between charge and spin degrees of freedom could explain the effect of a magnetic field on the slow relaxation properties where it was observed that a weak magnetic field has an effect on the relaxation time spectra [64].

Finally, it would be interesting to test the existence of slow dynamics effects in other types of experiments, such as dielectric response. Indeed, it is suggested in reference [50] that the residual so-called "β_0 process" could be the link to the low-T, slow heat relaxation phenomena. Dielectric experiments in the temperature range of 1 K and below are planned to test this hypothesis.

One of us (R.M.) acknowledges fruitful discussions on related topics with J.C. Anglès d'Auriac, F. Iglói and J. Souletie.

Appendix A: Weak ergodicity breaking in a REM-like trap model

In this Appendix we discuss a REM-like trap model having $p(E_\alpha) = p_0(E_\alpha) = \frac{1}{T_g} \exp(-E_\alpha/T_g)$ that was introduced in connection with the so-called "weak ergodicity breaking" property in reference [49]. We first recall in section A.1 the exact solution used by Bouchaud and Dean in reference [49] in their discussion of the weak ergodicity breaking property. We give in Section A.2 a set of approximations that can be used to recover the weak ergodicity breaking property. Similar approximations are used in the main body of the article (in Sect. 3) for the REM-like trap model of disordered CDWs. For this model relevant

to disordered CDWs it is not possible to use the same exact solution as Bouchaud and Dean and this is why we are lead to use a set of well controlled approximations.

A.1 Weak ergodicity breaking via an exact solution

The authors of reference [49] could demonstrate the so-called "weak ergodicity breaking" property in a model having $p(E_\alpha) = p_0(E_\alpha) = \frac{1}{T_g}\exp(-E_\alpha/T_g)$. We note $P_\alpha(t_w)$ the probability to find the system in trap α at time t_w. The evolution of the system is given by the Glauber dynamics [58]

$$\frac{\mathrm{d}}{\mathrm{d}t_w}P_\alpha(t_w) = -\sum_{\beta=1,\beta\neq\alpha}^{N} w_{\alpha\to\beta}P_\alpha(t_w) + \sum_{\beta=1,\beta\neq\alpha}^{N} w_{\beta\to\alpha}P_\beta(t_w), \quad \text{(A1)}$$

where the transition rates are given by $w_{\alpha\to\beta} = r_0\exp(-\beta E_\alpha)$ and $w_{\beta\to\alpha} = r_0\exp(-\beta E_\beta)$, with $\tau_0 = 1/r_0$ the microscopic time scale and $\beta = 1/T$ the inverse temperature. To solve equation (A1), it is convenient to make a Laplace transform with respect to the waiting time:

$$\tilde{P}_\alpha(E) = \int_0^{+\infty} E\mathrm{d}t_w \exp(-Et_w)P_\alpha(t_w).$$

In Laplace transform, the Glauber dynamics equation (A1) becomes

$$E\tilde{P}_\alpha(E) + Nr_0\mathrm{e}^{-\beta E_\alpha}\tilde{P}_\alpha(E) = \frac{E}{N} + \sum_\beta r_0\mathrm{e}^{-\beta E_\beta}\tilde{P}_\beta(E). \quad \text{(A2)}$$

The solution of equation (A2) is found to be

$$\tilde{P}_\alpha(E) = \frac{f_E(\tau_\alpha)}{\sum_\beta f_E(\tau_\beta)}, \quad \text{(A3)}$$

with $f_E(\tau_\alpha) = E\tau_\alpha/(1+E\tau_\alpha)$, and with $\tau_\alpha = \exp(\beta E_\alpha)/(Nr_0)$ the average trapping time in trap α. The expression of the Laplace transform of the dynamical correlation function is given by

$$\hat{\Pi}_0(t,E) = \int_0^{+\infty} p_0(E_\alpha)\tilde{P}_\alpha(E)\exp[-t/\tau_\alpha]\mathrm{d}E_\alpha. \quad \text{(A4)}$$

The presence of a dynamical glass transition can be seen from the divergence of the average relaxation time

$$\frac{\tau^{\mathrm{av}}}{\tau_0} = \langle\langle\frac{\tau_\alpha}{\tau_0}\rangle\rangle = \int_0^{+\infty} p_0(E_\alpha)\frac{\tau_\alpha}{\tau_0}\mathrm{d}E_\alpha = \frac{T}{T-T_g} \quad \text{(A5)}$$

while the typical relaxation time

$$\frac{\tau^{\mathrm{typ}}}{\tau_0} = \exp\left[\langle\langle\ln\left(\frac{\tau_\alpha}{\tau_0}\right)\rangle\rangle\right] = \exp\left[\frac{T_g}{T}\right] \quad \text{(A6)}$$

follows an Aharenius behavior. Using (A3), we obtain the correlation function

$$\hat{\Pi}_0(t,E) = \frac{\int_{\tau_0}^{+\infty} p_0(\tau)f_E(\tau)\mathrm{e}^{-t/\tau}\mathrm{d}\tau}{\int_{\tau_0}^{+\infty} p_0(\tau)f_E(\tau)\mathrm{d}\tau}\cdot \quad \text{(A7)}$$

The denominator can be evaluated by replacing $f_E(\tau)$ by $f_0(\tau)$ defined as $f_0(\tau) = E\tau$ if $\tau < 1/E$ and $f_0(\tau) = 1$ if $\tau > 1/E$. This leads to

$$\int_{\tau_0}^{+\infty} p_0(\tau)f_E(\tau)\mathrm{d}\tau \simeq \tau_0^{-T/T_g}\frac{1}{1-T/T_g} \times\left\{\frac{T_g}{T}(E\tau_0)^{T/T_g} - E\tau_0\right\}.$$

Since the waiting time is large compared to τ_0, one has $E\tau_0 \ll 1$ and therefore

$$\int_{\tau_0}^{+\infty} p_0(\tau)f_E(\tau)\mathrm{d}\tau \simeq \frac{T_g}{T(1-T/T_g)}E^{T/T_g}.$$

To evaluate the inverse Laplace transform of equation (A7), Bouchaud and Dean used the change of variable $u = f_E(\tau)$, from what they deduced the exact result

$$\Pi_0(t,t_w) = \frac{T}{T_g}\left(1-\frac{T}{T_g}\right)\int_{\frac{t}{t+t_w}}^{1}(1-u)^{T/T_g-1}u^{-T/T_g}\mathrm{d}u, \quad \text{(A8)}$$

which is valid if $T < T_g$. In the limiting cases $t/(t+t_w) \ll 1$ and $t/(t+t_w) \simeq 1$, equation (A7) reduces to

$$\Pi_0(t,t_w) \simeq 1 - \frac{T}{T_g}\left(\frac{t}{t+t_w}\right)^{1-T/T_g} \quad \text{if } t/(t+t_w) \ll 1 \quad \text{(A9)}$$

$$\Pi_0(t,t_w) \simeq \left(1-\frac{T}{T_g}\right)\left(\frac{t_w}{t+t_w}\right)^{T/T_g} \quad \text{if } t/(t+t_w) \simeq 1. \quad \text{(A10)}$$

The correlation function $\Pi_0(t,t_w)$ tends to zero if t_w is finite and $t \to +\infty$ while it tends to unity if t if finite and $t_w \to +\infty$, which constitutes the so-called "weak ergodicity breaking" property [49].

A.2 Weak ergodicity breaking via an approximate solution

Now let us give a set of approximations that can be used to recover the weak ergodicity breaking property. These approximations will be applied to another model in Section 3 in a situation where we cannot use the change of variable leading to (A8). The approximations are the following: (i) We replace $f_E(\tau)$ by $f_0(\tau)$ in the expression (A7) of $\hat{\Pi}_0(t,E)$; (ii) We replace the exponential

$\exp(-t/\tau)$ by the θ-function $\theta(\tau - t)$. We deduce the Laplace transform of the dynamical correlation function

$$\hat{\Pi}_0(t,E) \simeq 1 - \frac{T}{T_g}(Et)^{1-T/T_g} \text{ if } Et < 1 \quad \text{(A11)}$$

$$\hat{\Pi}_0(t,E) \simeq (1 - \frac{T}{T_g})(Et)^{-T/T_g} \text{ if } Et > 1. \quad \text{(A12)}$$

The inverse Laplace transform is evaluated within the same approximations. Namely we replace $\exp(-t/\tau_\alpha)$ by $\theta(\tau_\alpha - t)$. This leads to

$$\hat{\Pi}_0(t,E) \simeq \int_0^{1/E} E\mathrm{d}t_w \Pi_0(t,t_w),$$

from what we deduce

$$\Pi_0(t,t_w) = \frac{\partial}{\partial(1/E)}\left[\frac{\Pi_0(t,E)}{E}\right]_{E=1/t_w}.$$

The final form of the correlation function is found to be

$$\Pi_0(t,t_w) \simeq 1 - \left(\frac{T}{T_g}\right)^2 \left(\frac{t}{t_w}\right)^{1-T/T_g} \text{ if } t < t_w \text{ (A13)}$$

$$\Pi_0(t,t_w) \simeq \left[1 - \left(\frac{T}{T_g}\right)^2\right] \left(\frac{t_w}{t}\right)^{T/T_g} \text{ if } t_w < t. \text{ (A14)}$$

The approximate correlation functions given by (A13–A14) reproduce well the asymptotic behavior of the exact solution given by (A9–A10) except for the prefactors that are not relevant to our discussion. The qualitative physics of the model (namely the weak ergodicity breaking property) can thus be reproduced from these approximations. We use the same approximations in the main body of the article for the model having the trap energy distribution (3) for which we cannot use the exact solution anymore.

References

1. G. Parisi, Phys. Lett. A **73**, 203 (1979); M. Mézard, G. Parisi, N. Sourlas, G. Toulouse, M. Virasoro, Phys. Rev. Lett. **52**, 1156 (1984).
2. D.S. Fisher, D.A. Huse, Phys. Rev. Lett. **56**, 1601 (1986); D.S. Fisher, D.A. Huse, Phys. Rev. B **38**, 373 (1988).
3. A.J. Bray, M.A. Moore, *Heidelberg Colloquium on Glassy Dynamics and Optimization* Springer, Berlin (1986); A.J. Bray, M.A. Moore, Phys. Rev. Lett. **58**, 57 (1987).
4. M. Weissman, Rev. Mod. Phys. **65**, 829 (1993).
5. V. Dupuis, E. Vincent, J.P. Bouchaud, J. Hammann, A. Ito, H. Aruga Katori, Phys. Rev. B **64**, 174204 (2001); K. Jonason, E. Vincent, J. Hammann, J.P. Bouchaud, P. Nordblad, Phys. Rev. Lett. **81**, 3243 (1998); K. Jonason, P. Nordblad, E. Vincent, J. Hammann, J.P. Bouchaud, Eur. Phys. J. B **13**, 99 (2000).
6. J. Lamarcq, J.P. Bouchaud, O.C. Martin, M. Mézard, `cond-mat/0107544`.
7. J.P. Bouchaud, V. Dupuis, J. Hammann, E. Vincent, Phys. Rev. B **65**, 024439 (2002).
8. L.F. Cugliandolo, J. Kurchan, Phys. Rev. Lett. **71**, 173 (1993).
9. L. Berthier, J.L. Barrat, J. Kurchan, Eur. Phys. J. B **11**, 635 (1999); L. Berthier, Eur. Phys. J. B **17**, 689 (2000); L. Berthier, J.L. Barrat, J. Kurchan, Phys. Rev. Lett. **86**, 2014 (2001).
10. D.S. Fisher, P. Le Doussal, C. Monthus, Phys. Rev. Lett. **80**, 3539 (1998); P. Le Doussal, C. Monthus, D.S. Fisher, Phys. Rev. E **59**, 4795 (1999); D.S. Fisher, P. Le Doussal, C. Monthus, `cond-mat/0012290`.
11. S.K. Ma, C. Dasgupta, C.-K. Hu, Phys. Rev. Lett. **43**, 1434 (1979); C. Dasgupta, S.K. Ma, Phys. Rev. B **22**, 1305 (1980).
12. D.S. Fisher, Phys. Rev. Lett. **69**, 534 (1992); D.S. Fisher, Phys. Rev. B **51**, 6411 (1995).
13. D.S. Fisher, Phys. Rev. B **50**, 3799 (1994).
14. R.A. Hyman, K. Yang, R.N. Bhatt, S.M. Girvin, Phys. Rev. Lett. **76**, 839 (1996).
15. F. Iglói, H. Rieger, Phys. Rev. Lett. **78**, 2473 (1997); F. Iglói, H. Rieger, Phys. Rev. B **57**, 11404 (1998).
16. R.A. Hyman, K. Yang, Phys. Rev. Lett. **78**, 1783 (1997).
17. C. Monthus, O. Golinelli, Th. Jolicœur, Phys. Rev. Lett. **79**, 3254 (1997).
18. O. Motrunich, S.-C. Mau, D.A. Huse, D.S. Fisher, Phys. Rev. B **61**, 1160 (2000).
19. R. Mélin, Y.-C. Lin, P. Lajkó, H. Rieger, F. Iglói, preprint (2001).
20. M. Hase, K. Uchinokura, R.J. Birgeneau, K. Hirota, G. Shirane, J. Phys. Soc. Jpn **65**, 1392 (1996); M. Hase, N. Koide, K. Manabe, Y. Sasago, K. Uchinokura, A. Sawa, Physica B **215**, 164 (1995).
21. M.C. Martin, M. Hase, K. Hirota, G. Shirane, Phys. Rev. B **56**, 3173 (1997).
22. T. Masuda, A. Fujioka, Y. Uchiyama, I. Tsukada, K. Uchinokura, Phys. Rev. Lett. **80**, 4566 (1998).
23. K. Manabe, H. Ishimoto, N. Koide, Y. Sasago, K. Uchinokura, Phys. Rev. B **58**, R575 (1998).
24. Y. Ichiyama, Y. Sasago, I. Tsukuda, K. Uchinokura, A. Zheludev, T. Hayashi, N. Miura, P. Boni, Phys. Rev. Lett. **83**, 632 (1999).
25. D.J. Buttrey, J.D. Sullivan, A.L. Rheingold, J. Solid. State Chem. **88**, 291 (1990).
26. B. Batlogg, S.W. Cheong, L.W. Rupp Jr, Physica B **194-196**, 173 (1994).
27. J.F. DiTusa, S.W. Cheong, J.H. Park, G. Aeppli, C. Broholm, C.T. Chen, Phys. Rev. Lett. **73**, 1857 (1994).
28. K. Kojima, A. Keren, L.P. Lee, G.M. Luke, B. Nachumi, W.D. Wu, Y.J. Uemura, K. Kiyono, S. Miyasaka, H. Takagi, S. Uchida, Phys. Rev. Lett. **74**, 3471 (1995).
29. C. Payen, E. Janod, K. Schoumacker, C.D. Batista, K. Hallberg, A.A. Aligia, Phys. Rev. B **62**, 2998 (2000).

30. V. Villar, R. Mélin, C. Paulsen, J. Souletie, E. Janod, C. Payen, Eur. Phys. J. B **25**, 39 (2002).
31. D. Khomskii, W. Geertsma, M. Mostovoy, Czech. J. Phys. **46** (1996), Suppl. S6, LT21 Conference Proceedings.
32. B. Grenier, J.P. Renard, P. Veillet, C. Paulsen, R. Calemcsuk, G. Dhalenne, A. Revcolevschi, Phys. Rev. B **57**, 3444 (1998).
33. M. Saint-Paul, J. Voiron, C. Paulsen, P. Monceau, G. Dhalenne, A. Revcolevschi, J. Phys. Cond. Matt. **10**, 10215 (1998).
34. A. Dobry, P. Hansen, J. Riera, D. Augier, D. Poilblanc, Phys. Rev. B **60**, 4065 (1999).
35. M. Laukamp, G.B. Martins, C. Gazza, A.L. Malvezzi, E. Dagotto, P.M. Hansen, A.C. López, J. Riera, Phys. Rev. B **57**, 10755 (1998).
36. P.M. Hansen, J.A. Riera, A. Delia, E. Dagotto, Phys. Rev. B **58**, 6258 (1998).
37. P. Hansen, D. Augier, J. Riera, D. Poilblanc, Phys. Rev. B **59**, 13557 (1999).
38. E. Sorensen, I. Affleck, D. Augier, D. Poilblanc, Phys. Rev. B **58**, R14701 (1998).
39. T. Kennedy, J. Phys. Cond. Matt. **2**, 5737 (1990).
40. M. Hagiwara, K. Katsumata, I. Affleck, B.I. Halperin, J.P. Renard, Phys. Rev. Lett. **65**, 3181 (1990).
41. E. S. Sørensen, I. Affleck, Phys. Rev. B **51**, 16115 (1995).
42. S. Yamamoto, S. Miyashita, Phys. Rev. **50**, 6277 (1994).
43. R.N. Bhatt, P.A. Lee, Phys. Rev. Lett. **48**, 344 (1982).
44. M. Fabrizio, R. Mélin, Phys. Rev. Lett. **78**, 3382 (1997); M. Fabrizio, R. Mélin, Phys. Rev. B **56**, 5996 (1997); M. Fabrizio, R. Mélin, J. Phys. Cond. Matt. **9**, 10429 (1997); M. Fabrizio, R. Mélin, J. Souletie, Eur. Phys. J. B **10**, 607 (1999); R. Mélin, Eur. Phys. J. B **18**, 263 (2000).
45. R. Mélin, Eur. Phys. J. B **16**, 261 (2000).
46. K. Biljaković, F. Nad, J.C. Lasjaunias, P. Monceau, K. Bechgaard, J. Phys. Cond. Matt. **6**, L135 (1994); K. Biljaković, F. Nad, J.C. Lasjaunias, P. Monceau, K. Bechgaard, Synth. Met. **71**, 1849 (1995); J.C. Lasjaunias, K. Biljaković, P. Monceau, Phys. Rev. B **53**, 7699 (1996).
47. J.C. Lasjaunias, K. Biljaković, D. Staresinic, P. Monceau, S. Takasaki, J. Yamada, S. Nakatsuji, H. Anzai, Eur. Phys. J. B **7**, 541 (1999).
48. K. Biljaković, J.C. Lasjaunias, P. Monceau, F. Levy, Phys. Rev. Lett. **62**, 1512 (1989); K. Biljaković, J.C. Lasjaunias, P. Monceau, F. Levy, Phys. Rev. Lett. **67**, 1902 (1991).
49. J.P. Bouchaud, J. Phys. I France **2**, 1705 (1992); J.P. Bouchaud, E. Vincent, J. Hamman, J. Phys. I France **4**, 139 (1994); J.P. Bouchaud, D.S. Dean, J. Phys. I France **5**, 265 (1995); C. Monthus, J.P. Bouchaud, J. Phys. A **29**, 3847 (1996).
50. D. Staresinić, K. Biljacović, W. Brütting, K. Hosseini, P. Monceau. H. Berger, F. Levy, Phys. Rev. B in press (2002).
51. S. Sahling, J.C. Lasjaunias, P. Monceau, A. Revcolevschi, Solid State Commun. **92**, 423 (1994).
52. K. Efetov, A.I. Larkin, Zh. Eksp. Teor. Fiz. **72**, 2350 (1977); K. Efetov, A.I. Larkin, Sov. Fiz. JETP **45**, 1236 (1977).
53. A.I. Larkin, P. Lee, Phys. Rev. B **17**, 1596 (1978).
54. S. Brasovskii, *Charge Density waves*, edited by L. Gorkov, G. Grüner (Elsevier, Amsterdam, 1990).
55. A.I. Larkin, Zh. Eksp. Teor. Fiz. **105**, 1793 (1994); A.I. Larkin Sov. Fiz. JETP **78**, 971 (1994).
56. Yu. N. Ovchinikov, K. Biljakovic, J.C. Lasjaunias, P. Monceau, Europhys. Lett. **34**, 645 (1996).
57. B. Derrida, Phys. Rev. B **24**, 2613 (1981); B. Derrida, G. Toulouse, J. Phys. Lett. **46**, L223 (1985).
58. R.J. Glauber, J. Math. Phys. **4**, 294 (1963).
59. V. Kiryukin, B. Keimer, J.P. Hill, A. Vigliante, Phys. Rev. Lett. **76**, 4608 (1996).
60. M. Horvatić, Y. Fagot-Revurat, C. Berthier, G. Dhalenne, A. Revcolevschi, Phys. Rev. Lett. **83**, 420 (1999).
61. R. Mélin, J. Phys. I France **6**, 469 (1996); R. Mélin, P. Butaud, J. Phys. I France **7**, 691 (1997).
62. F. Alberrici-Kious, J.P. Bouchaud, L.F. Cugliandolo, P. Doussineau, A. Levelut, Phys. Rev. Lett. **81**, 4987 (1998).
63. J. Riera, D. Poilblanc, Phys. Rev. B **63**, 241102 (2001).
64. J.C. Lasjaunias, S. Sahling, K. Biljacović, P. Monceau, unpublished.